ACS OMEGA

http://pubs.acs.org/journal/acsodf

Article

Contactless Method of Emulsion Formation Using Corona Discharge

Amir Dehghanghadikolaei, Mohcen Shahbaznezhad, Bilal Abdul Halim, and Hossein Sojoudi*

Cite This: *ACS Omega* 2022, 7, 7045−7056

Read Online

ACCESS | Metrics & More | Article Recommendations | Supporting Information

ABSTRACT: Electroemulsification methods use electrohydrodynamic (EHD) forces to manipulate fluids and droplets for emulsion formation. Here, a top-down method is presented using a contactless corona discharge for simultaneous emulsion formation and its pumping/collection. The corona discharge forms using a sharp conductive electrode connected to a high-voltage source that ionizes water vapor droplets (formed by a humidifier) and creates an ionic wind (electroconvection), dragging them into an oil medium. The nonuniform electric field induced by the corona discharge also drives the motion of the oil medium via an EHD pumping effect utilizing a modulated bottom electrode geometry. By these two effects, this contactless method enables the immersion of the water droplets into the moving oil medium, continuously forming a water-in-oil (W/O) emulsion. The impact of corona discharge voltage, vertical and horizontal distances between the two electrodes, and depth of the silicone oil on sizes of the formed emulsions is studied. This is a low-cost and contactless process enabling the continuous formation of the W/O emulsions.

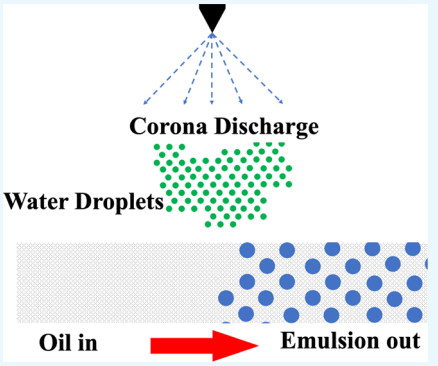

1. INTRODUCTION

Emulsions are stable mixtures of two naturally immiscible liquids dispersed into each other uniformly or nonuniformly, enabling the presence of a continuous phase and a dispersed phase sitting together, typically using a surfactant.[1] Emulsions can be found in different categories of water-in-oil (W/O) and oil-in-water (O/W) and different subcategories of water-in-oil-in-water (W/O/W) and oil-in-water-in-oil (O/W/O) in sizes ranging from macro- to nano- to microemulsions.[2−4] Although the terms micro and nano should refer to sizes of larger and smaller droplets in scale, respectively, in the science of emulsion, microemulsions consist of smaller droplets when compared to nanoemulsions.[5] The size range of droplets dispersed in the continuous phase of different emulsions could be arranged on the order of 0.5−100 μm for macroemulsions, 0.1−1 μm for nanoemulsions, and 0.01−0.1 μm for microemulsions.[6] In general, the most important parameters that play a role in determining the range of droplet sizes in an emulsion are the chemical and physical characteristics of the dispersed and continuous phases. The physical properties include viscosity, temperature, density, and electrical/thermal conductivity.[7] Among chemical properties, the polarity of the dispersed and continuous phases play a major role in the stability of the formed emulsions.[8]

As a rule of thumb, emulsification processes require four different elements, which are continuous phases (water or oil), dispersed phases (oil or water), energy for emulsification (ultrasonic vibration, temperature changes, chemical reactions, pressure variations, etc.), and finally a connecting compound that acts as an emulsifier (different types of water-soluble or oil-soluble surfactants).[9−12] The commercially available emulsion formation processes are distinguished first by their level of energy consumption and then by the different activation sources of the emulsification processes. For the first sorting criteria, the emulsification processes are categorized into two distinct groups of high-energy and low-energy methods with approximate energy consumptions of 10^8−10^{10} and 10^3−10^5 W/kg, respectively.[13] From the high-energy methods, high-pressure (or ultra-high-pressure) homogenization[14] and ultrasonic emulsification[15] are the most common ones, while membrane and microchannel emulsification are used as well.[16,17] On the other hand, the most utilized low-energy methods are phase inversion processes (phase inversion temperature and phase inversion composition) and spontaneous emulsification.[18,19] Each of the introduced categories of emulsion formation processes has its advantages and disadvantages. As an instance, the high-energy methods consume significantly higher energy and produce considerably larger emulsion droplets while they require less emulsifier agents.[20] However, the low-energy methods are extremely sensitive to the composition of the continuous and dispersed phases and the temperature that drives the emulsion formation process, while they produce noticeably smaller emulsion droplets.[21] Another drawback of the low-energy emulsification methods is the need for high concentration of emulsifier agents that alter the chemical

Received: November 30, 2021
Accepted: February 4, 2022
Published: February 18, 2022

https://doi.org/10.1021/acsomega.1c06765
ACS Omega 2022, 7, 7045−7056

Table 1. Nominal Properties of the Silicone Oil and Water Used in the Emulsion Formation Experiments[32]

liquid	density, ρ (g/cm^3)	kinematic viscosity, ν (cSt)	electrical conductivity, σ (S/m)	surface tension, γ (mN/m)	relative permittivity, ϵ
silicone oil	0.964	100	1×10^{-13}	20.9	2.73
water	0.996	1	16×10^{-4}	72.8	80.1

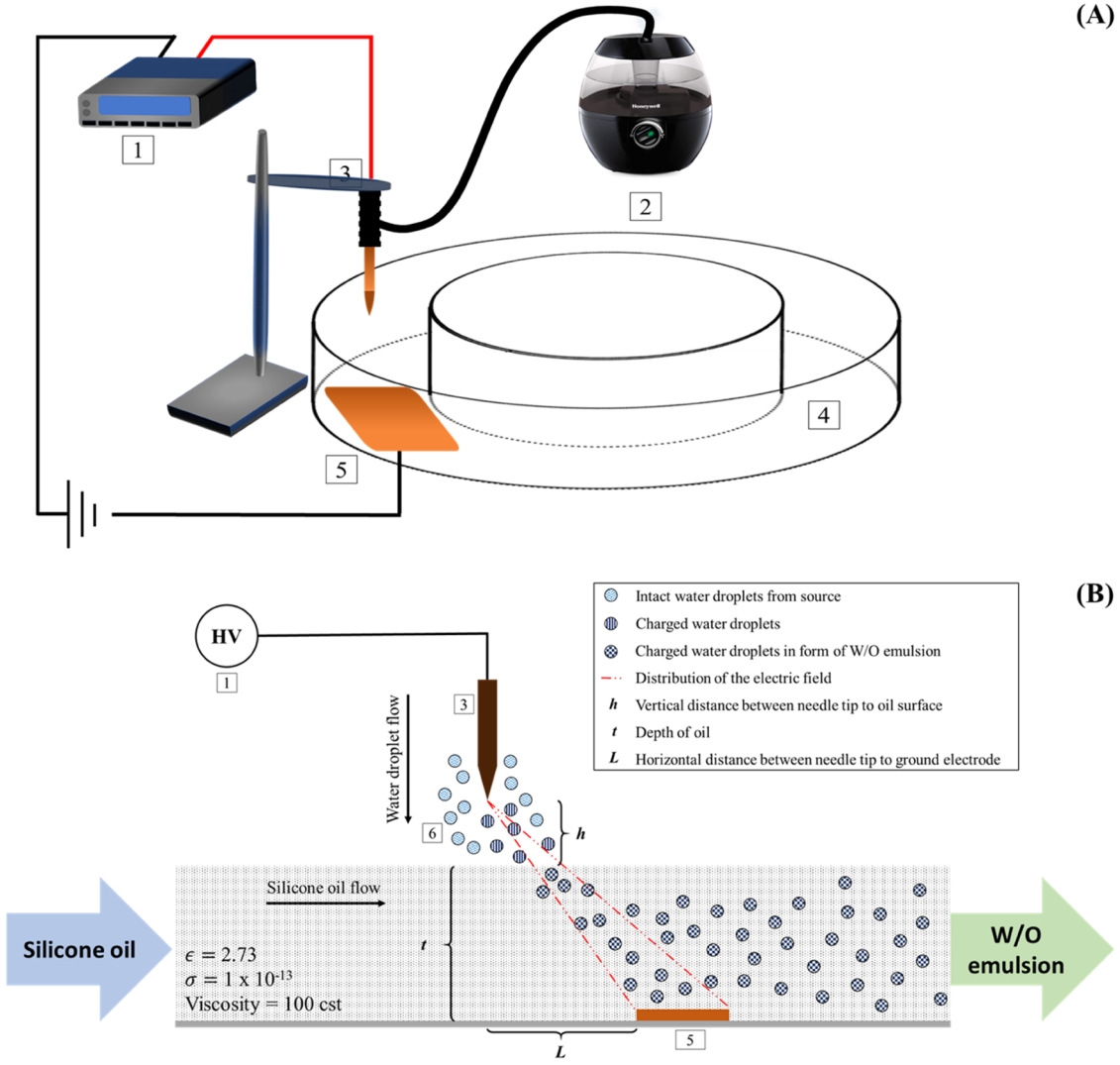

Figure 1. Schematic representation of the emulsion formation process via corona discharge. (1) High-voltage power supply equipped with an amplifier and a function generator, (2) a homestyle humidifier, (3) a sharp tungsten needle electrode, (4) a transparent circular pump, (5) a ground counter electrode made of copper, and (6) the water droplets accelerating down toward the oil surface. (A) Major components of the process. (B) Various phenomena during the emulsion formation process. Water droplets formed by the humidifier are charged via the corona discharge, accelerating toward, and diffusing into the oil medium. Electrohydrodynamic (EHD) pumping of the oil induced by the corona discharge enables its continuous exposure to the water droplets and formation and collection of the emulsion on the other side of the circular pump (5).

properties of the final products. This could turn unsafe and undesired, especially for skin and cosmetic applications.[22] In addition, hydrophilic−lipophilic balance (HLB), critical micelle concentration (CMC), viscosity, and density of the continuous and dispersed phases limit the types of the emulsions that can be made using low-energy methods.[23]

Although all of the discussed methods have shown promise for industrial applications, they introduce common limitations. Alteration of chemical properties, due to a high concentration of surfactants or high processing temperature, and change of physical properties, due to high mechanical pressure in combination, along with the inability for continuous production of emulsions are among the most common difficulties that the commercially available emulsification methods represent.[24,25] To overcome these deficiencies, electroemulsification methods could be a proper alternative solution. In these processes, the liquid media are not in contact with any external mechanical disturbance and the applied electric field does the task of liquid manipulation. Although the experimental conditions have to meet certain constraints, flexibility of the electroemulsification processes enables the use of different liquids as continuous and dispersed phases.[26] However, caution should be accounted for while using volatile and flammable oils.[25] Due to this flexibility, it has been feasible to produce engineered W/O/W and O/W/O emulsions with selective chemical compositions, droplet sizes, and viscosities for different applications with significantly less

https://doi.org/10.1021/acsomega.1c06765
ACS Omega 2022, 7, 7045−7056

Table 2. Combinations of Process Parameters for Four Different Groups Studied in This Work and Qualitative Chances of Cone Formation for Each Distinct Process Parameter

	Chance of cone formation						Combination of the parameters
Process parameter							
Voltage, V (kV)	10	9	8	7	6		h = 15 mm, L = 20 mm, t = 8 mm
Vertical distance, h (mm)	10	15	20	25	30	35	V = 10 kV, L = 20mm, t = 8mm
Horizontal distance, L (mm)	5	10	15	20	25	30	V = 8 kV, h = 15 mm, t = 8 mm
Oil thickness, t (mm)	2	3.5	5	6.5	8		V = 8 kV, h+t = 23 mm, L = 20 mm
	← *Higher chances*			*Lower chances* →			

energy consumption when compared to the mechanical agitation methods.[27] In addition, the previous works on electroemulsification claim that due to the existence of the built-up charges in the dispersed phase, the overall stability and shelf life of the emulsions are increased.[28] However, the disadvantage of electric field-based processes is that in a certain combination of process parameters, electrocoalescence (reverse process of electroemulsification or separation of emulsion) takes place, producing larger dispersed phase droplets. Some modifications such as the use of magnetic stirrer and rotary drums have been implemented to alleviate the electrocoalescence, but they do not provide practical solutions for real applications, especially on large scales.[28,29]

Here, a novel contactless configuration of electroemulsification is presented, utilizing a corona discharge for simultaneous emulsion formation and its continuous pumping/collection. Corona discharge forms when a high-potential electric field is discharged through a single point toward a counter electrode. Corona discharge is a branch of cold plasma discharge with a slightly visible fainted blue color that becomes more visible when the applied electric field intensifies.[30] The media around the sharp conductive electrode (i.e., air or inert gases) become ionized, forming an ionic wind that accelerates toward the counter electrode. This nonthermal discharge has many applications where the media underneath are sensitive to temperature changes.[31]

A sharp conductive electrode (tungsten needle) is connected to a high voltage for forming a nonuniform electric field via the negative corona discharge. The negative corona discharge ionizes the air molecules around the electrode (discharge zone), creating an ionic wind that carries water droplets (formed by a humidifier) toward a silicone oil medium. A ground electrode (plate) is placed inside the oil medium leading to oil circulation via electrohydrodynamic (EHD) pumping, without impacting its viscosity. The water droplets drift toward the circulating oil and immerse into it due to electroconvection, continuously forming a W/O emulsion. The offset of the ground electrode to the surface beneath the ionizing electrode is engineered to obtain the desired motion of the continuous phase (i.e., silicone oil) for efficient emulsion formation. The effect of different working parameters such as voltage (V), vertical distance of the sharp needle tip to the oil surface (h), horizontal distance of the needle tip to the start of the ground electrode (L), and the depth of the silicone oil (t) on the properties of the W/O emulsion are investigated. This study paves the path for developing a contactless, continuous, and power-efficient method for the production of W/O emulsions with potential applications in the cosmetics, drug delivery, and food industries[32−35] (see Table 1).

2. RESULTS AND DISCUSSION

Here, the corona discharge is utilized to accelerate ionized water droplets (formed by the humidifier) and diffuse them into a silicone oil medium that is circulating inside the designed pump due to the electrohydrodynamic (EHD) effect induced by the corona discharge. Figure S1 shows a simple EHD pump with alumina particles that are carried in the oil/flow due to the corona discharge. This process results in the formation of W/O emulsions. As a high-potential electric field is applied to the needle, a nonuniform electric field forms above and inside the silicone oil medium. The electric field distribution is in the form of a cone with its tip at the needle tip and its base at the surface of the ground electrode (placed in the bottom of the silicone oil). Depending on the strength of the applied electric field, positioning of the two electrodes relative to each other, and the electrical resistance in the path between them, the applied EHD forces change. As a result, the silicone oil might deform instead of only circulating inside the pump. Although there are many different configurations for nonuniform electric field generation, the pin-to-plate setup was selected since it has been widely used and it does not have specific mechanical constraints or processing limits (e.g., Joule heating, etc.).[36,37]

The impact of four different processing parameters on the properties of the W/O emulsions made of 100 cSt silicone oil is studied. The highest and the lowest thresholds of the processing parameters were experimentally found for each set of parameters. The applied high voltage (V) was set to start from +6 kV with increments of 1 kV until reaching a maximum of +10 kV. The vertical distance between the sharp tungsten needle/electrode and the top surface of the silicone oil (h) was set to be 10 mm and reached a maximum of 35 mm with increments of 5 mm. The horizontal distance between the tip of the sharp needle/electrode and the starting edge of the ground electrode (L) was set to start from 5 mm, reaching a maximum of 30 mm with increments of 5 mm. Finally, the depth of the silicone oil (t) was calculated from its initial mass, starting from 1.5 mm and reaching 8 mm with increments of 2 mm. Figure 1 shows these processing parameters, and Table 2 summarizes their corresponding values. On the other hand, the effect of electrostatic fields and forces, the interaction of static charges on each other and the process, and how they behave under different processing parameters could be an interesting idea to explore. Although the charges are in constant motion toward the electrodes (based on their charge sign), many of them statically exist in the ionization

https://doi.org/10.1021/acsomega.1c06765
ACS Omega 2022, 7, 7045−7056

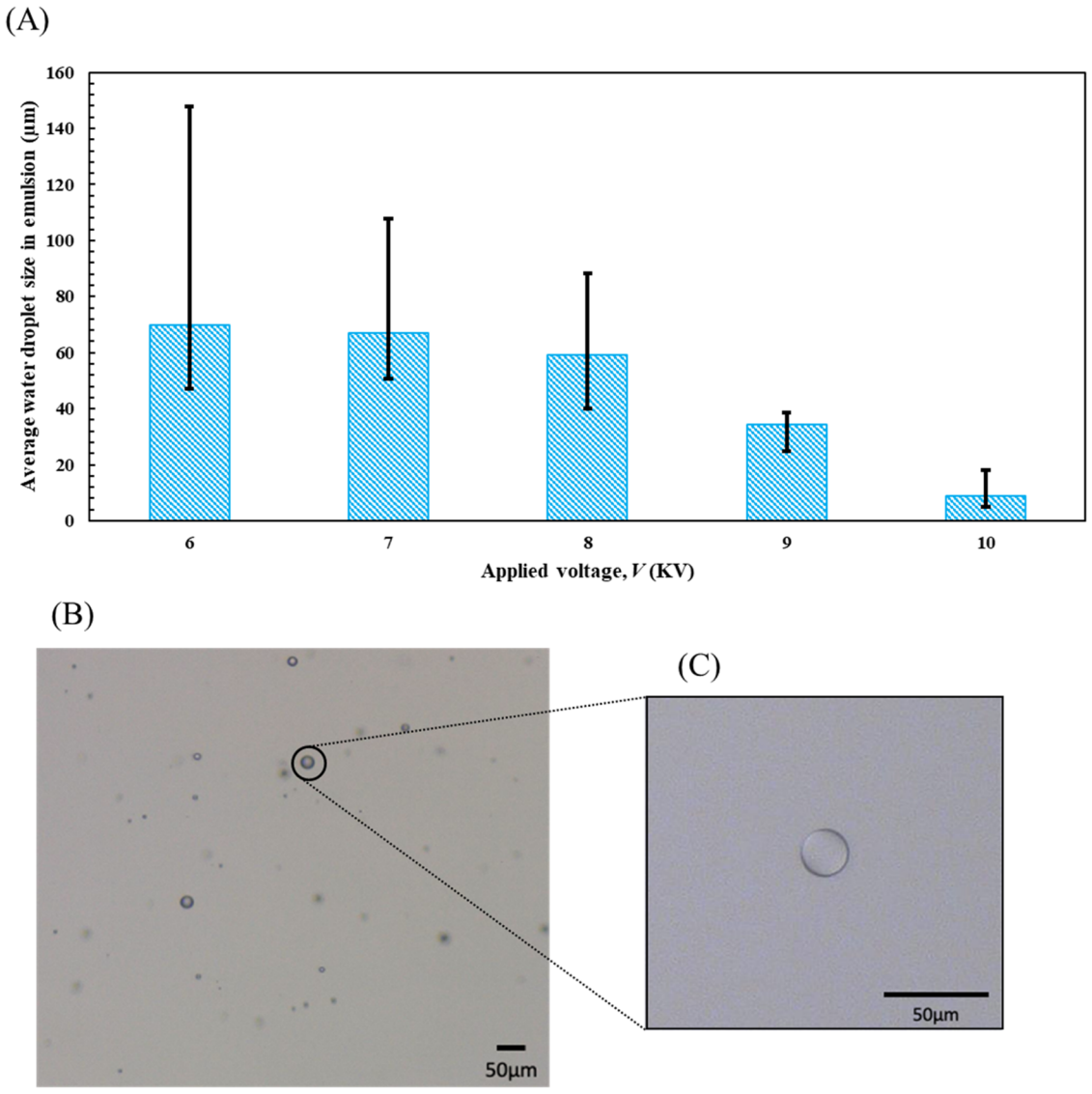

Figure 2. Impact of the applied voltage (V) on the size of the water droplets in the emulsions. The experiments were performed on 100 cSt silicone oil mixed with 1 wt % of a Span 80 surfactant agent under a constant vertical distance of h =15 mm, a horizontal distance of L = 20 mm, and a depth of oil of t = 8 mm, and voltage varying between +6 and +10 kV in +1 kV increment. (A) The average water droplet sizes for different voltage levels. An increase in the applied voltage leads to a more uniform emulsion with smaller size droplets. (B) A representative optical microscopy (OM) of the emulsion formed under +10 kV applied voltage. (C) A high-resolution OM image showing water droplets as small as a couple of micrometers in the emulsion.

region, which will have a direct effect on the flux of the moving charges. A brief discussion of the static charges and electrostatic forces is presented in the Supporting Information, but a more in-depth discussion on the effect of electrostatic fields and forces would be discussed elsewhere. Figure S2 represents a schematic of the ionization process and the interaction of the charges and particles under corona discharge.

2.1. Impact of Voltage (V) on the Average Size of the Water Droplets in the Emulsion. When the voltage is applied to the sharp conductive needle, it creates ions due to the existence of a high-potential gradient, the so-called "corona discharge". The corona discharge also ionizes the water droplets formed by the humidifier. These ions drift toward the ground electrode forming an ionic wind that carries ionized water droplets toward the ground electrode that is placed inside the oil medium. This phenomenon is called electroconvection that leads to diffusion of the water droplets inside the oil. A simple electroconvection process is presented in Video S2, which shows the behavior of the humidity (water droplets) flow before and after applying the corona discharge, without the presence of any oil medium. With increasing the voltage, the induced electric field intensifies accelerating the charged particles (i.e., water droplets) toward the counter (ground) electrode further. On the other hand, the applied voltage to the needle forms a nonuniform electric field in a cone-shaped distribution. This nonuniform electric field along with ions drifting toward the ground electrode induces electrohydrodynamic forces inside the oil medium.[38] Knowing that the neutral medium (silicone oil before applying any external electric field) is stationary, the resulting EHD forces for positively and negatively charged particles/ions could be calculated (see eqs S1−S3). It turns out that the EHD forces are in direct correlation to the current density applied to the discharge region ($F_{EHD} \propto$ current density).[39] In this set of experiments, the distance between the two electrodes (on the other hand, h and L) and the depth of oil (t) were kept constant, translating to a constant initial electrical

https://doi.org/10.1021/acsomega.1c06765
ACS Omega 2022, 7, 7045−7056

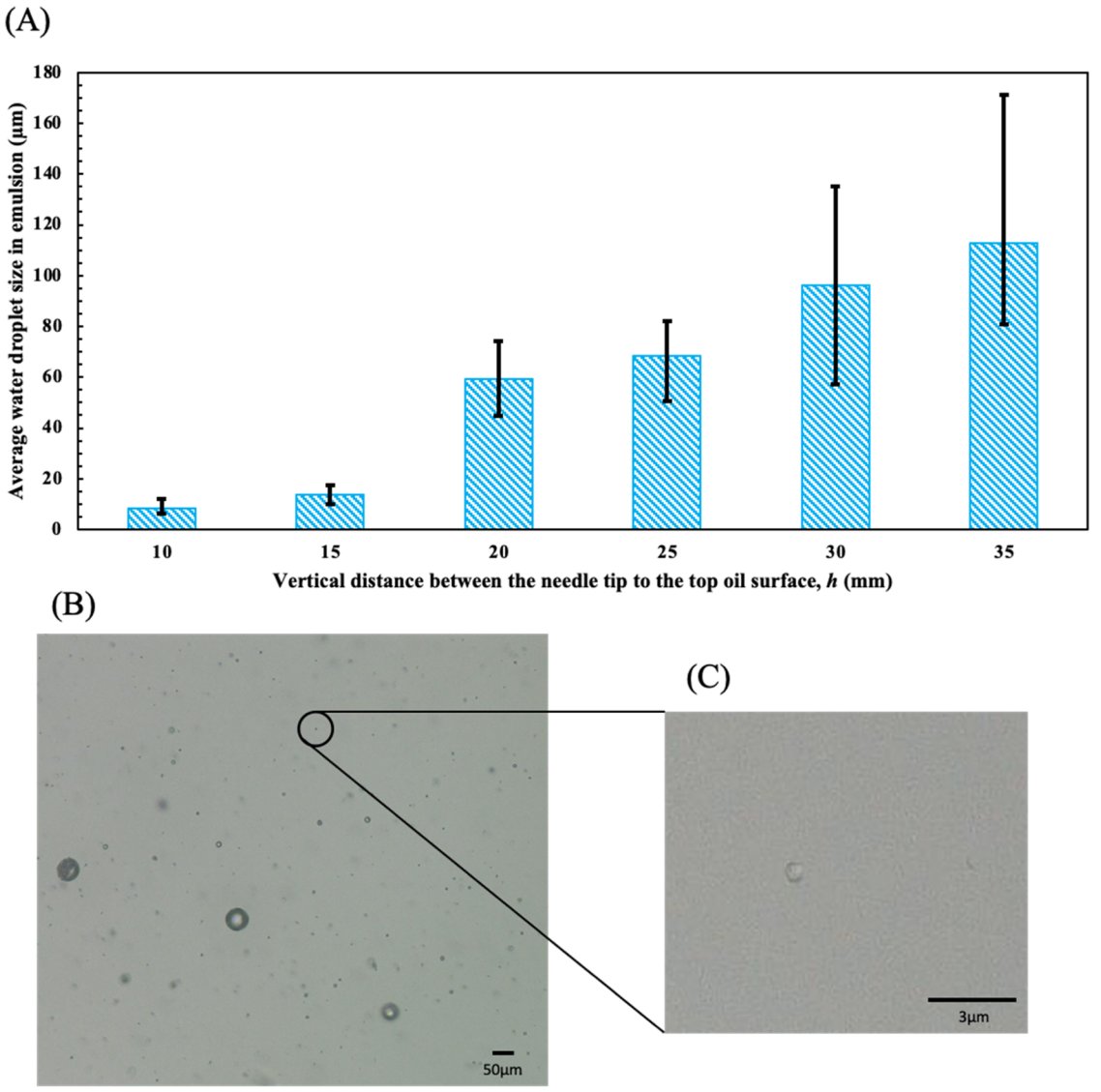

Figure 3. Impact of the vertical distance between the tip of the sharp electrode and the top of the oil surface (h) on the size of water droplets in the emulsions. The experiments were performed on silicone oil with 100 cSt viscosity mixed with 1 wt % of a Span 80 surfactant agent under a constant horizontal distance of L = 20 mm, a voltage of V = +10 KV, a depth of oil of t = 8 mm, and vertical distance varying between 10 and 35 mm with 5 mm increments. (A) The average water droplet sizes for different vertical distances. With a decrease in the vertical distance, the emulsion becomes more uniform with smaller-sized water droplets. (B) A representative optical microscopy (OM) of the emulsion formed under a vertical distance of h = 10 mm. (C) A high-resolution OM image showing water droplets as small as a couple of micrometers in the emulsion.

resistance for all experiments (before applying any voltage). However, since the corona discharge follows Townsend's discharge law, in the glow discharge region (where the corona discharge lies), an increase in voltage leads to a decrease in the current density. This behavior is valid up to the initial arc discharge regions.[40−42] Therefore, because of increased current density, the number of charged ions moving toward the ground electrode increases, consequently intensifying the EHD forces.

During the emulsification process via corona discharge, the ionized water droplets accelerate toward the ground electrode that is placed inside the silicone oil medium. Since the accelerating water droplets have the same sign of charges (i.e., positive), they tend to repel each other within the oil medium due to Coulombic forces, enhancing the stability of the formed emulsion.[43] However, in some cases, either due to a nonuniform size of the water droplets formed by the humidifier or due to a lower oil circulation velocity, some droplets get trapped close to the ground electrode. While the trapped droplets bounce up and down between the free oil surface and the ground electrode, they consume the newly entered water droplets and transform into larger droplets.[44,45] The disadvantage of having larger droplets is that they get heavier as their mass augments and they sediment quickly. As a result, the EHD force applied to these droplets does not overcome their resistance to move into the direction of the flow and further coalescence takes place. While this process continues to occur, the quality of the emulsion deteriorates as well as its stability. Due to this phenomenon, in lower voltages (in which the EHD forces are weaker), the average size of the water droplets in the emulsion increases. It is hypothesized that some of the water droplets might not have enough charge and/or momentum to pass the surface tension and diffuse into the oil medium upon impact. This can lead to coalescence of these droplets with enhanced sizes, momenta, and charges (due to continuous impact of the electric field) that can then diffuse into

https://doi.org/10.1021/acsomega.1c06765
ACS Omega 2022, 7, 7045−7056

the oil medium. The ultimate outcome is the formation of emulsions with droplet sizes of 8−12 μm in diameter that is several times larger than the sizes of the feed water droplets (~1.62 μm). The average size of the water droplets in the emulsions formed under various voltages is presented in Figure 2.

In Figure 2, the working voltage was increased from +6 to +10 kV with increments of +1 kV. The threshold voltage for the onset of corona discharge was set at +6 kV since the motion of the silicone oil was observed to be extremely slow at lower voltages to a point that at +4 kV there was no visible motion. As a result, the lower voltages were not included in the results. On the other hand, +10 kV is the maximum voltage that the power supply was able to provide. The combination of other parameters for this set of experiments was as follows: the vertical distance of the needle to the top oil surface, h = 15 mm, the horizontal distance between the needle tip to the start of the ground electrode, L = 20 mm, and a depth of silicone oil, t = 8 mm. In the emulsion formed using +10 kV voltage, the velocity of the oil circulation was the highest due to a stronger EHD force (see Video S3). When the oil/emulsion circulation velocity is high, the water droplets do not have a chance to experience any coalescence as diffused to the medium. Gradually, as the voltage was decreased, the velocity was decreased, and the time needed for the oil/emulsion to fully circulate increased. This decrease in the circulation velocity provided enough time for the existing water droplets to discharge and obtain neutral or opposite charges, leading to coalescence with newly diffused water droplets as the emulsification process continues. Therefore, the average size of the water droplets in the collected emulsion is increasing with a decrease in the applied voltage. At the same time, the margin of the smallest and the largest measured water droplets (the error bar) is also increasing drastically. This leads to less uniform emulsion formation, which is due to the coexistence of the newly added droplets (smallest ones) and previously coalesced droplets (largest ones). For example, the emulsion formed using +6 kV voltage has water droplets varying from 40 to 150 μm in size. Finally, we observe that applied voltages of +9 kV and above are more desirable for the formation of uniform W/O emulsions with smaller-sized water droplets.

2.2. Impact of Vertical Distance (h) on the Average Size of the Water Droplets in the Emulsion. Intensity of a nonuniform electric field induced by the corona discharge is inversely proportional to the distance between the two electrodes ($E \propto h^{-2}$) (see eqs S4 and S5).[46,47] As the distance between the two electrodes increases, the intensity of the electric field formed by a constant applied voltage decreases with a second-order magnitude. Figure 3 represents the average size of the water droplets in the W/O emulsion formed under various vertical distances of the electrodes (h). The combination of the processing parameters for this set of experiments was as follows: a voltage of V = +10 kV, the horizontal distance between the electrodes of L = 20 mm, a depth of oil of t = 8 mm, and one round of oil circulation to form an emulsion in all experiments. The vertical distance between the electrodes (h) was changed from 10 to 35 mm with 5 mm increments. When the vertical distance is 10 and 15 mm, the average droplet sizes in the emulsion are close, but as the vertical distance increases, a significant increase in the droplet size was observed. Simultaneously, the emulsion becomes more nonuniform with wider ranges between the smallest and the largest droplets. Overall, with a decrease in the vertical distance, the intensity of the electric field under a given applied voltage increases, leading to faster oil/emulsion circulation that does not provide enough chance for the droplets to coalesce. This leads to smaller-sized water droplets and more uniform emulsion formation. The applied electric field generates EHD forces, which have two components in vertical and horizontal directions, $F_{EHD\cdot y}$ and $F_{EHD\cdot x}$, respectively. As the horizontal and vertical distances, or their combination, change during the experiments, the overall acting forces change as well. Depending on the relative position of the two electrodes, the circulation velocity induced via different acting forces changes. An increase in the vertical distance (h) changes the angle at which the EHD forces are applied to the oil surface. For instance, in a vertical distance of h = 35 mm, a semiperpendicular force is applied to the oil, which has a significantly larger vertical component when compared to its horizontal one. Consequently, the overall force is not effective enough to drive the medium (i.e., oil and/or W/O emulsion) forward. This simply reflects in the lower circulation of the medium and an emulsion with significantly larger water droplets.

When the vertical distance increases, the intensity of the electric field becomes weaker resulting in slower circulation velocity of the oil/emulsion. This leads to entrapment of the water droplets between the two electrodes and their consequent electrocoalescence. The motion of the smaller trapped droplets is governed by an effect of the electric field, which is known as electrophoretic (EP) force.[48] After several bounces between the top surface of the oil and the ground electrode, the electrocoalescence increases the size of the droplets.[49,50] Considering Coulomb's law, the larger droplets with a larger surface area need more EP force to continue their bouncing behavior and their speed of reciprocation will decrease.[51] The EP force could be easily calculated using $F_{EP} = E \cdot Q$, where E is the intensity of the electric field and Q is the charge on the surface of the droplets. As the droplets become larger, their charge density on the surface is decreased and consequently the generated EP forces are decreased leading to enhanced entrapment of the droplets.[52] In addition to the change in charge density and magnitude of the EP forces, the drag force is changing as well. As the water droplets get larger in dimension, the resisting drag force increases, which further hinders their free motion in the continuous phase. The correlation between the drag force and the size of the water droplets is linear ($f_d \propto$ size of droplets; see eq S6).[53]

Overall, reduced EP forces and enhanced drag forces lead to reduction in the mobility of droplets as they become larger due to coalescence. Ultimately, the large droplets escape from the intense electric field zone (underneath the needle) circulating with the oil/emulsion.[54] However, these varying phenomena lead to the formation of a wide range of water droplet sizes when vertical distances are high. The significant increase in the size of the droplets by an increase in the vertical distance when compared to an increase in the applied voltage could be related to first-order vs second-order dependences of the electric field (E) to V, and h, respectively.

2.3. Impact of Horizontal Distance (L) on the Average Size of the Water Droplets in the Emulsion. Changing the horizontal distance between the two electrodes changes the intensity of the electric field, EHD forces, and consequently the size of the water droplets in the emulsion. Increasing the horizontal distance (L) is a key factor in decreasing the angle of the overall EHD forces on the oil surface. However, unlike the effect of the vertical distance, by increasing L, the average size of the water droplets does not follow an absolute inclining or declining trend. Figure 4 shows the variation of the change in

https://doi.org/10.1021/acsomega.1c06765
ACS Omega 2022, 7, 7045−7056

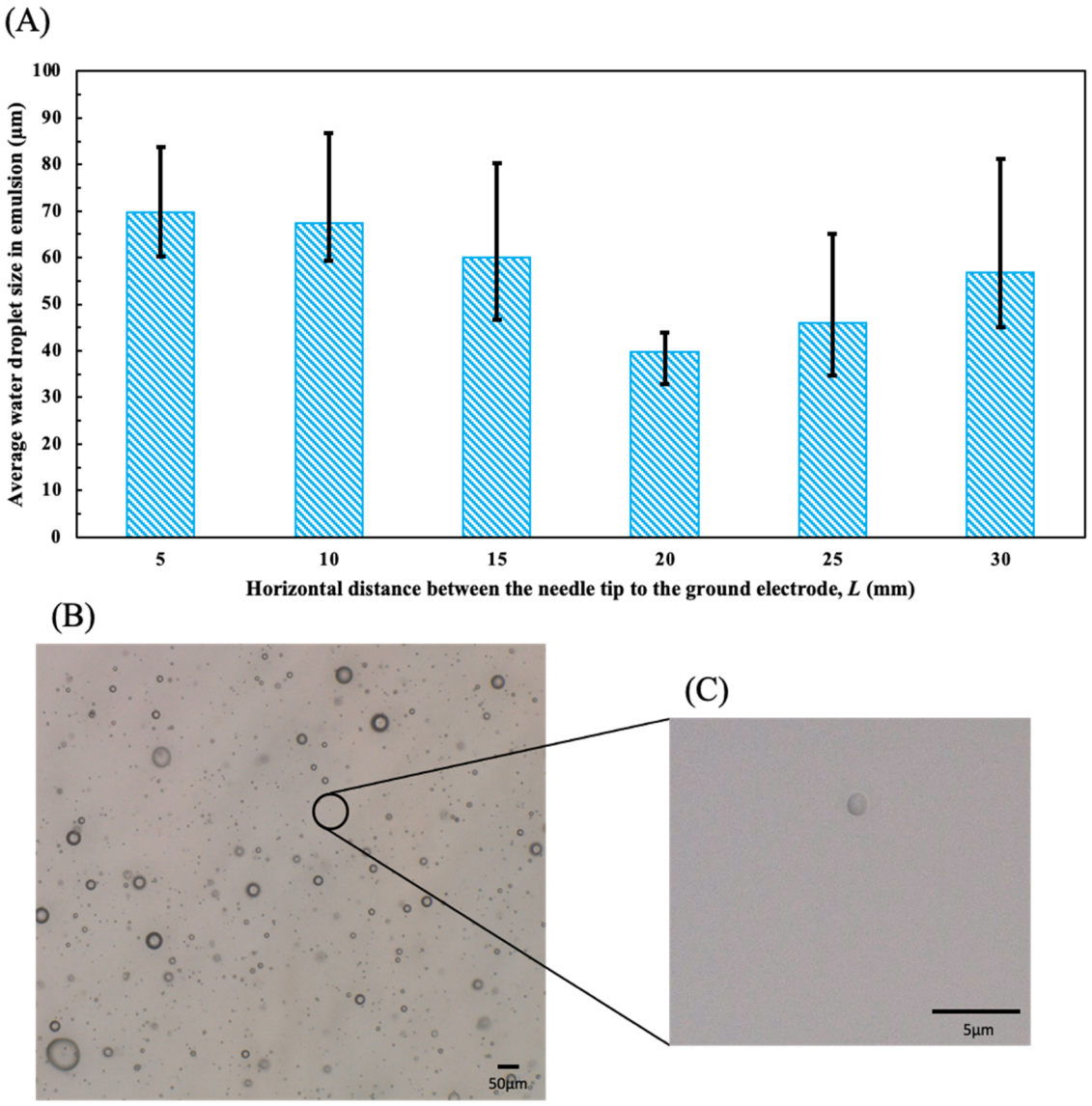

Figure 4. Impact of the horizontal distance between the tip of the sharp electrode to the starting point of the ground electrode (L) on the size of water droplets in the emulsions. The experiments were performed on 100 cSt silicone oil mixed with 1 wt % of a Span 80 surfactant agent under a constant voltage of V = +8 kV, a vertical electrode distance of h = 15 mm, a depth of oil of t = 8 mm, and one round of processing with the horizontal distance varying between 5 and 30 mm in increments of 5 mm. (A) The average water droplet sizes for different horizontal distances. By a constant increase in the values of the horizontal distance, the average size of the water droplets was decreased to a point and after that it started increasing again. (B) A representative optical microscopy (OM) of the emulsion formed under 20 mm of horizontal distance. (C) A high-resolution OM image showing water droplets as small as a couple of micrometers in the emulsion.

water droplet size under different conditions. The processing conditions for this set of experiments were as follows: a voltage of V = +8 kV, a vertical distance between the two electrodes of h = 15 mm, a depth of oil of t = 8 mm, and one round of circulation for all of the experiments. The horizontal distance between the electrodes, L, was increased with increments of 5 mm from 5 to 30 mm.

As can be seen from Figure 4, with increasing the horizontal distance, the average size of the droplets is decreasing. However, this trend is only valid until the horizontal distance reaches L = 20 mm. After this point, the average size of the droplets is increasing once more. In horizontal distances of L < 20 mm, the effect of the electric field is more inclined vertically (i.e., the EHD forces are acting in the vertical direction). In these conditions, the EHD forces do not act in the direction of circulating the oil/emulsion within the pump and instead squeeze the oil downward, leading to Taylor cone formation. This cone formation causes a vortex, which interrupts the oil/emulsion circulation leading to entrapment of the droplets in the intensely discharged zone right underneath the needle. Overall, water droplets experience enhanced coalescence and become larger. For the horizontal distances of L > 20 mm, the intensity of the electric field and consequently its resulting EHD forces are considerably decreased. It is hypothesized that lower EHD forces lead to lower oil/emulsion circulation velocity that provides enough time for the droplets to coalesce, increasing their overall sizes.

Warburg's law, on the other hand, indicates that the existing current density on the surface of a dielectric is changing with a change in the angle between the tip of the needle and a point on the surface of the dielectric.[55,56] This law presents a threshold for discharge angle within which the electric field has an effective

https://doi.org/10.1021/acsomega.1c06765
ACS Omega 2022, 7, 7045−7056

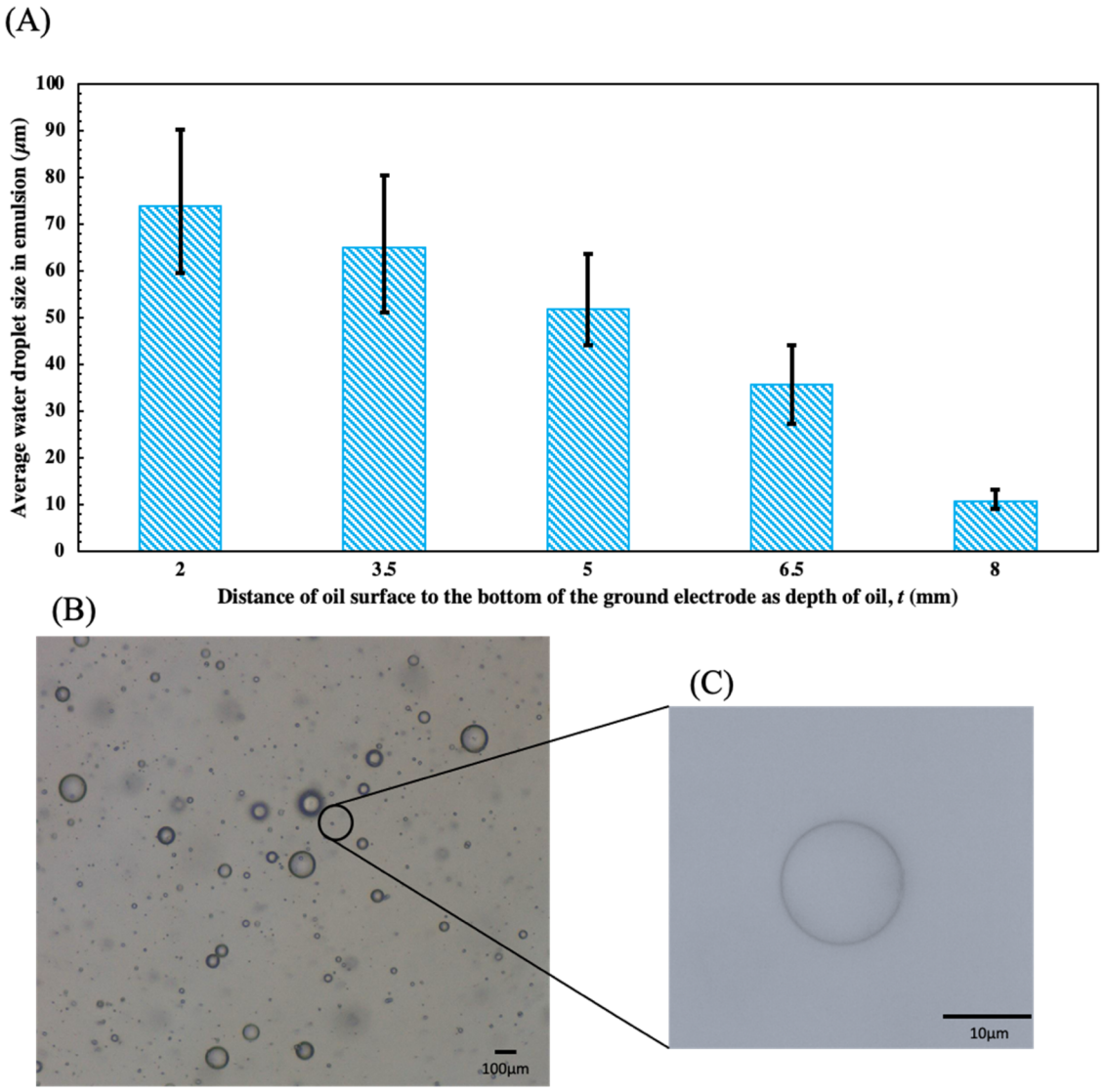

Figure 5. Impact of the depth of oil in the pump (t) on the average size of the water droplets in the formed emulsions. The experiments were performed on 100 cSt silicone oil mixed with 1 wt % of a Span 80 surfactant agent under a voltage of V = +8 kV, a horizontal electrode distance of L = 20 mm, an initial vertical electrode distance of h = 15 mm, and a depth of oil varying between 2 and 8 mm in increments of 1.5 mm. It should also be noted that the $h + t$ value was kept constant at 23 mm during these experiments. (A) The average water droplet size for different depths of oil. With decreasing the depth of oil, the average size of the droplets increases constantly. The increasing trend of the droplet size is uniformly positive throughout the experiments. (B) A representative optical microscopy (OM) of the emulsion formed under a depth of oil of t = 8 mm. (C) A high-resolution OM image showing water droplets as small as a couple of micrometers.

intensity. Passing this threshold, the horizontal component of the EHD forces gets smaller to a point that there would be no forward motion induced. At the maximum horizontal distance of 30 mm, $\theta \approx 63°$, which is in the threshold of the angles introduced by Warburg's law ($\theta \leq 65°$). Since higher horizontal distances increase the discharge angle to higher than the introduced threshold, L = 30 mm was selected as the highest horizontal distance of the experiments (see eq S7 for the mathematical representation of Warburg's law).

2.4. Impact of Depth of Oil (t) on the Average Size of the Water Droplets in the Emulsion. The last studied parameter is the effect of depth of oil or the height of the silicone oil from the surface of the ground copper electrode to the top surface of the oil (see Figure 1). Like the other parameters, a change in the depth of oil (t) results in alterations in oil/emulsion behavior between the two electrodes, which itself influences the electroemulsification characteristics. Although the EHD forces are influencing the manipulation of the injected water droplets into the silicone oil, other mechanisms are involved in determining the ultimate size of the water droplets inside the formed W/O emulsion. Figure 5 shows the average size of water droplets inside the emulsions formed under various depths of oil (t) with a combination of other parameters as a voltage of V = +8 kV, an initial vertical distance of h = 15 mm, a horizontal distance of L = 20 mm, and one round of processing. The depth of oil (t) was varying between 2 and 8 mm with 1.5 mm increments. It should be noted that the initial vertical distance of h = 15 mm was measured from the top surface of the oil in a depth of t = 8 mm (it was set to a constant value of 23 mm from the tip of the needle to the surface of the ground electrode). Consequently, by decreasing the depth of oil (t), the vertical distance (h) was changed in increments of 1.5 mm. The distance between the needle tip and the bottom surface of the oil remained constant (see Figure 1).

https://doi.org/10.1021/acsomega.1c06765
ACS Omega 2022, 7, 7045−7056

As shown in Figure 5, the average size of the droplets is increasing, while the depth of oil is decreased. The medium within the discharge region consisted of air (with water droplets) and silicone oil, both imposing electrical resistances. By decreasing the depth of oil, the thickness of the air layer between the two electrodes increases. Although the electrical conductivity of ionized air in the discharge region is significantly high, with an increase in the discharge distance (changing the depth of oil), the current density of the discharge regime decreases, which results in a weaker discharge (see Section 2.2).[57] As the discharge gets weaker, a partial ionization takes place in front of the needle, which leaves some portion of air intact. Consequently, an increased air thickness results in a slightly increased electrical resistance ($R_t = R_{\text{partially-ionized air}} + R_{\text{silicone oil}}$).[58]

As the discharge starts, the charged objects move toward the opposing electrode. However, in the initial stages of the discharge, the charged objects get trapped on the surface of the oil layer due to the electric resistance. This causes a gradual increase in the electric pressure behind the resisting layers, which is reflected in the increase of current density. When this condition is met, a sudden discharge of the charged particles rapidly goes toward the opposing electrode.[59] After this breakdown point, the discharge continues since the high-potential electrode is constantly feeding the charged objects.[60,61] On the other hand, the electrostatic pressure (p) is in square relation with the intensity of the electric field or number of charged objects ($p \propto E^2$) (see eq S8). With excessive electrostatic pressure in locally stronger electric fields, the surface of the dielectric deforms severely to a point that it forms deep cones, which in severe cases reach the surface of the ground electrode (see Figure S3). In this situation, there would be a short circuit that does not provide any EHD pumping through the liquid and consequently no emulsification process occurs.[32,62]

In lower depths of oil, as the electric resistance slightly increases, the number of the trapped charges on the oil surface increases, which consequently enhances the electric pressure on its surface. As the surface of the oil was forcibly deformed due to the increased electric pressure, the charged water droplets finally found their way toward the ground copper electrode by forming a cone (cone depth depends on the depth of oil). When the depth of oil is low enough, a deep cone formation occurs, which causes a vortex in the silicone oil. This vortex interrupts the circulation of the oil and results in electrocoalescence of water droplets instead of forming emulsions. Based on the observations during the experiments, the cone formation takes place in the middle of the pumping channel, which allows a weak oil flow in the areas around the cone. Depending on the size of the cones, the velocity of the flow around them is variable. In some extreme conditions, the flow is not guaranteed, especially at lower depths of oil and higher voltages. With the increased size of cones, the droplets get trapped permanently around the cones, resulting in an infinite increase in water droplet size up to a point that there are two distinct phases of water and oil visible in the pumping setup. Due to this, the acting voltage of this set of experiments was set to $V = +8$ kV (instead of +10 kV) to prevent such a phenomenon. Figure S3 shows the vortices from which a high disturbance in the circulation flow occurs and even some portions of the fluid locally try to move in the opposite direction. Although the backward flow is not permanent, it significantly reduces the circulation velocity of the silicone oil and consequently the uniformity of the final emulsion.

In the 12 distinct steps of a vortex formation (Figure S3), it can be clearly seen that once a vortex is born, it remains in a different form or intensity but its entity and effect on the flow remain throughout the process. In the initial steps, the surface of the oil is deformed due to the electrostatic pressure of the charges. Once the pressure surpasses the surface tension, a deep vortex in the shape of a cone forms, which consequently generates undesired flows before and after its location.[63] The disturbed flow behind the vortex is the one that extremely affects the desired flow of the fluid in the pump. As illustrated, the disturbed flows before and after the vortex remain as long as the vortex is in action. Microscopic images shown in Figures 2−5 are just representatives of several images taken from each type of emulsion. Droplet sizes with error bars are obtained from the average of several different images/measurements. In addition, the appearance of larger water droplets can be partially due to coalescence of the smaller ones (sometimes even before entering the oil medium).

Finally, the power consumption rate of corona emulsification is calculated and compared to that of traditional methods. To this end, the corona current (I_c) is measured and multiplied by the applied voltage (V) to obtain the power (P). For a W/O emulsion made under operating parameters of $L = 20$ mm, $t = 8$ mm, $h = 15$ mm, and $V = +10$ kV, the obtained power is ∼3.8 W. This is 2 orders of magnitude lower than the power consumption rate of emulsification via mechanical methods (i.e., ultrasonic emulsification or high-pressure homogenization).[64−66] Future studies can focus on better understanding the power consumption rate of the corona emulsification and its optimization. This can lead to tuning the emulsion formation parameters/processes for efficiently obtaining a desired emulsion.

3. CONCLUSIONS

A contactless method to form W/O emulsion using a corona discharge is introduced. The corona discharge creates (1) an electroconvection to carry water droplets and diffuse them into an oil medium and (2) an electrohydrodynamic (EHD) that pumps/circulates the oil during the diffusion of the water droplets. Impact of operating voltage, depth of the silicone oil, and electrode configuration on the sizes of the formed emulsion is investigated.

It is found that the operating corona voltage significantly impacts the circulation/pumping speed of the oil, leading to drastic changes in the sizes of the water droplets inside the emulsion. Higher voltages were found to be favorable for fast oil circulation and formation of uniform and fine-sized W/O emulsions. The combination of vertical and horizontal distances between two opposing electrodes is found to be crucial for preventing oil deformation (Taylor cone formation) and entrapment of the diffused water droplets beneath the electrodes. This led to customized uniformity and sizes of the formed emulsions. Modulating the electrical resistances between the two opposing electrodes via combined effects of the depth of silicone oil and the needle height led to controlled emulsion formation. Given the limitations of operating parameters in this study, it is found that the applied voltage of $V = +10$ kV, the vertical distance of $h = 15$ mm, the horizontal distance of $L = 20$ mm, and the depth of oil of $t = 8$ mm leads to the formation of fine-sized and uniform W/O emulsions. Overall, it was found that for emulsion formation the operating parameters need to be adjusted in a way that cone formation is avoided. This study paves the path for a low-cost process,

https://doi.org/10.1021/acsomega.1c06765
ACS Omega 2022, 7, 7045−7056

enabling the continuous production of W/O emulsions. Future studies can focus on studying the impact of corona discharge on the formation of other types of emulsions (i.e., micro- and/or nanoemulsions) and on developing algorithms to obtain best-operating conditions for such emulsion formation processes. Surface tension, viscosity, and dielectric constant of the oil may affect the property of the formed emulsion, which can be explored in future studies.

4. MATERIALS AND METHODS

Silicone oil with a kinematic viscosity of 100 cSt (μ MicroLubrol, Clifton, NJ) was used for emulsion formation (see Table 1 for details).[32] To enhance the emulsification process, 1 wt % of Span 80 surfactant (Sigma-Aldrich, St. Louis, MO) was added to the silicone oil medium. After addition of the surfactant, the product was shaken gently and then it was mixed ultrasonically with a digital ultrasonic cleaner (Vevor, Los Angeles, CA) for three rounds of 15 min with 30 min intervals to allow sufficient cooling. The high potential required for corona discharge formation was provided by a power supply (Siglent, Solon, OH), which is capable of producing up to 1000 V in both alternating and direct current modes (AC and DC). The output potential of the power supply was then entered to a high-voltage amplifier (Advanced Energy, Lockport, NY) to get a 10× output (up to 10 kV). Throughout the experiments, the electrical characteristics of the process were controlled with the same function generator. A sharp tungsten needle electrode (Bovie Medical Corporation, Clearwater, FL) with a tip diameter of ≈65 μm was attached to the high-voltage end of the power supply and countered by a copper ground electrode (SparkFun Electronics, Boulder, CO) to form the corona discharge in the region between the two electrodes. The vertical and horizontal distances of the needle tip to the top of the silicone oil surface and front edge of the ground copper electrode were measured carefully using a set of markings and fixed steel gauges. To measure the height of the silicone oil in the Petri dish, the mass of the added oil was measured using a precision digital scale (US Solid, Cleveland, OH). Knowing the density of the silicone oil, the mass was then converted into the height of the liquid for each experiment. A homestyle humidifier (Honeywell, Charlotte, NC) was utilized to form water droplets. The size of the water droplets was measured to be ≈1.62 μm in diameter using an environmental particulate matter sensor SPS 30 (Sensirion, Staefa, Switzerland) with a lower limit detection of 0.3 μm (see Figure S1). The output of the humidifier was connected to a tube in line with the sharp tungsten needle to allow ionization and acceleration of the water droplets via the corona discharge.

The pumping container was made of two transparent Petri dishes connected concentrically via an instant glue to make a circular channel for guiding of raw silicone oil and processed products (W/O emulsions). Since lighter water droplets tend to float on the top surface of oil and the heavier ones more likely sediment to its bottom, the emulsion sample collection was carried out from different regions of the container consistently. The collected samples were mixed in a single glass vial before any characterization to ensure that the collected samples represent an average size of all introduced water droplets. In a stationary configuration, the stabilized water droplets under the discharge get trapped and consume the newly added droplets and consequently form a larger one, which is not desired. To be consistent, a processing time equal to the time consumed for the fastest circulation was set for all of the experimental combinations. In the case of this study, the fastest time of one round of circulation was measured by adding alumina particles to the raw oil and letting it circulate a complete round, which was measured to be ∼53 s. This time was then set to be the basis for conducting all other experiments. However, in lower velocity samples (depending on the combination of the processing parameters), the considered time was not sufficient to achieve emulsion formation in the entire medium of the silicone oil. As a result, the scheme of the experiments was changed to let each sample pass one complete round of circulation. Figure 1A represents a schematic illustration of the setup.

Since some of the samples were circulating slower when compared to the fastest one, they did not pass one complete round of the circulation at the given time, and as a result, some portions of the silicone oil in those samples were not treated with the corona discharge. To cancel the negative effect of collecting untreated samples on the average size of the droplets, oil portions were manually collected from four different spots from both the top and bottom of the product medium, with a pipet. Then, the samples were transferred to a glass vial and were prepared for optical microscopy on quartz microscopic slides. The process of imaging was done using a digital microscope (Keyence Corporation of America, Itasca, IL). After imaging, the raw digital files were deployed to ImageJ to get the binary output of the droplets detected in the field of view. Using the imaging scale bar and the size of the pixels in each binary image, the size of the droplets was calculated using a Python script. The average sizes of the water droplets were calculated seven times for each sample to obtain the highest level of certainty in the results.

The EHD pumping in the silicone oil is a result of the external nonuniform electrical force applied to the surface of the silicone oil. As a result of this force, the top surface of the silicone oil undergoes different levels of deformation from slightly concaved (downward) to severely deformed, forming a deep cone (Taylor cone), which sometimes exposes the surface of the copper ground electrode to the air based on the severity of the deformation.[67] Based on our previous study on the same setup, the desired experimental combination for emulsion formation parameters should prevent occurring of any major deformation in the oil.[32] This situation is commonly seen while the processing parameters are at their highest extreme values (i.e., at very high voltage) where the EHD forces are maximized.[68] The Taylor cone formation phenomenon (see Figure S3) was closely observed with an Olympus i-Speed 3 high-speed camera (iX Cameras, Rochford, Essex, U.K.). On the other hand, when the combination of the parameters moves to the lowest level of EHD forces, the motion in the fluid becomes as slow that it could be neglected. Since water has higher electrical conductivity compared to air, while the humidity runs between the two electrodes, the tuned processing parameters do not respond as desired.[58] As a result, one more round of experiments was done to offset the starting and ending points of each processing parameter. To have such a viable range of processing parameters, each separate parameter was examined for both extremes (lowest and highest) of the EHD forces. Using this method of extremum, it was possible to figure out the two ends of the parameters for each set of experiments without numerous experiments. Figure 1B represents a schematic overview of the emulsification process. The red dashed lines indicate the region that the electric field has a sensible power to cause EHD pumping. The same region is where the severe deformation of the liquid surface takes place (cone formation).

https://doi.org/10.1021/acsomega.1c06765
ACS Omega 2022, 7, 7045−7056

■ ASSOCIATED CONTENT

Supporting Information

The Supporting Information is available free of charge at https://pubs.acs.org/doi/10.1021/acsomega.1c06765.

Discussion about the equations used to qualitatively describe the phenomena occurring during the emulsion formation process with corona discharge; equations S1−S8 represent simplified EHD force calculations for charged particles, the relation of electric field intensity and its variables, and the electrostatic pressure exerted to the system from the electric fields; and furthermore, Figures S1−S3 represent the mist droplet size (diameter) and schematic of the ionization process in addition to the sequences of cone formation during the process (PDF)

EHD pumping (Video S1) (MP4)

Behavior of the mist with and without the presence of the corona discharge (Video S2) (MP4)

Comparison of three different oil circulation velocities (Video S3) (MP4)

■ AUTHOR INFORMATION

Corresponding Author

Hossein Sojoudi − *Department of Mechanical, Industrial, and Manufacturing, The University of Toledo, Toledo, Ohio 43615, United States;* orcid.org/0000-0002-5278-9088; Email: Hossein.Sojoudi@utoledo.edu

Authors

Amir Dehghanghadikolaei − *Department of Mechanical, Industrial, and Manufacturing, The University of Toledo, Toledo, Ohio 43615, United States*

Mohcen Shahbaznezhad − *Department of Electrical Engineering and Computer Science, The University of Toledo, Toledo, Ohio 43615, United States*

Bilal Abdul Halim − *Department of Mechanical, Industrial, and Manufacturing, The University of Toledo, Toledo, Ohio 43615, United States*

Complete contact information is available at: https://pubs.acs.org/10.1021/acsomega.1c06765

Notes

The authors declare no competing financial interest.

■ ACKNOWLEDGMENTS

The authors cordially thank the University of Toledo machine shop and John Jaegly for his help in preparing the setup for safely conducting high-voltage experiments.

■ REFERENCES

(1) Kale, S. N.; Deore, S. L. Emulsion micro emulsion and nano emulsion: a review. *Syst. Rev. Pharm.* **2016**, *8*, 39.

(2) Anton, N.; Vandamme, T. F. Nano-emulsions and micro-emulsions: clarifications of the critical differences. *Pharm. Res.* **2011**, *28*, 978−985.

(3) Hou, W.; Xu, J. Surfactant-free microemulsions. *Curr. Opin. Colloid Interface Sci.* **2016**, *25*, 67−74.

(4) Hejazifar, M.; Lanaridi, O.; Bica-Schröder, K. Ionic liquid based microemulsions: A review. *J. Mol. Liq.* **2020**, *303*, No. 112264.

(5) Jiménez Saelices, C.; Capron, I. Design of Pickering micro-and nanoemulsions based on the structural characteristics of nanocelluloses. *Biomacromolecules* **2018**, *19*, 460−469.

(6) Solans, C.; Izquierdo, P.; Nolla, J.; Azemar, N.; Garcia-Celma, M. J. Nano-emulsions. *Curr. Opin. Colloid Interface Sci.* **2005**, *10*, 102−110.

(7) Vargaftik, N. B. *Handbook of Physical Properties of Liquids and Gases − Pure Substances and Mixtures*; Springer, 1975.

(8) Boucher, E.; Murrell, J. *Properties of Liquids and Solutions*; Wiley, 1982.

(9) Modarres-Gheisari, S. M. M.; Gavagsaz-Ghoachani, R.; Malaki, M.; Safarpour, P.; Zandi, M. Ultrasonic nano-emulsification−A review. *Ultrason. Sonochem.* **2019**, *52*, 88−105.

(10) Salehi, F. Physico-chemical and rheological properties of fruit and vegetable juices as affected by high pressure homogenization: A review. *Int. J. Food Prop.* **2020**, *23*, 1136−1149.

(11) Jhalani, A.; Sharma, D.; Soni, S. L.; Sharma, P. K.; Sharma, S. A comprehensive review on water-emulsified diesel fuel: chemistry, engine performance and exhaust emissions. *Environ. Sci. Pollut. Res.* **2019**, *26*, 4570−4587.

(12) Tadros, T. F. *Emulsion Formation, Stability, and Rheology*; Wiley, 2013; pp 1−75.

(13) McClements, D. J.; Jafari, S. M. Improving emulsion formation, stability and performance using mixed emulsifiers: A review. *Adv. Colloid Interface Sci.* **2018**, *251*, 55−79.

(14) Gali, L.; Bedjou, F.; Velikov, K. P.; Ferrari, G.; Donsì, F. High-pressure homogenization-assisted extraction of bioactive compounds from Ruta chalepensis. *J. Food Meas. Charact.* **2020**, *14*, 2800−2809.

(15) Taha, A.; Ahmed, E.; Ismaiel, A.; Ashokkumar, M.; Xu, X.; Pan, S.; Hu, H. Ultrasonic emulsification: An overview on the preparation of different emulsifiers-stabilized emulsions. *Trends Food Sci. Technol.* **2020**, *105*, 363−377.

(16) Liu, Y.; Li, Y.; Hensel, A.; Brandner, J. J.; Zhang, K.; Du, X.; Yang, Y. A review on emulsification via microfluidic processes. *Front. Chem. Sci. Eng.* **2020**, *14*, 350−364.

(17) Joscelyne, S. M.; Trägårdh, G. Membrane emulsification—a literature review. *J. Membr. Sci.* **2000**, *169*, 107−117.

(18) Solans, C.; Morales, D.; Homs, M. Spontaneous emulsification. *Curr. Opin. Colloid Interface Sci.* **2016**, *22*, 88−93.

(19) Preziosi, V.; Perazzo, A.; Caserta, S.; Tomaiuolo, G.; Guido, S. Phase Inversion Emulsification. *Chem. Eng. Trans.* **2013**, *32*, 1585−1590.

(20) Patrignani, F.; Lanciotti, R. Applications of high and ultra high pressure homogenization for food safety. *Front. Microbiol.* **2016**, *7*, No. 1132.

(21) Jasmina, H.; Džana, O.; Alisa, E.; Edina, V.; Ognjenka, R. Preparation of Nanoemulsions by High-Energy and Low Energy Emulsification Methods. In *CMBEBIH 2017*; Springer, 2017; Vol. *62*, pp 317−322.

(22) Yang, Y.; Marshall-Breton, C.; Leser, M. E.; Sher, A. A.; McClements, D. J. Fabrication of ultrafine edible emulsions: Comparison of high-energy and low-energy homogenization methods. *Food Hydrocolloids* **2012**, *29*, 398−406.

(23) Maffi, J. M.; Meira, G. R.; Estenoz, D. A. Mechanisms and conditions that affect phase inversion processes: A review. *Can. J. Chem. Eng.* **2021**, *99*, 178−208.

(24) Jaworek, A. Electrostatic micro-and nanoencapsulation and electroemulsification: a brief review. *J. Microencapsulation* **2008**, *25*, 443−468.

(25) Karyappa, R. B.; Naik, A. V.; Thaokar, R. M. Electro-emulsification in a uniform electric field. *Langmuir* **2016**, *32*, 46−54.

(26) Rozynek, Z.; Bielas, R.; Józefczak, A. Efficient formation of oil-in-oil Pickering emulsions with narrow size distributions by using electric fields. *Soft Matter* **2018**, *14*, 5140−5149.

(27) Mun, S.; Decker, E. A.; McClements, D. J. Influence of droplet characteristics on the formation of oil-in-water emulsions stabilized by surfactant− chitosan layers. *Langmuir* **2005**, *21*, 6228−6234.

(28) Nawab, M.; Mason, S. The preparation of uniform emulsions by electrical dispersion. *J. Colloid Sci.* **1958**, *13*, 179−187.

(29) Hughes, J.; Pavey, I. Electrostatic emulsification. *J. Electrost.* **1981**, *10*, 45−55.

(30) Adamiak, K.; Atten, P. Simulation of corona discharge in point−plane configuration. *J. Electrost.* **2004**, *61*, 85−98.

(31) Sigmond, R.; Goldman, M. *Corona Discharge Physics and Applications*; NATO Advanced Study Institute (ASI), 1983; p 1.

(32) Mohamed, M. H.; Shahbaznezhad, M.; Dehghanghadikolaei, A.; Haque, M. A.; Sojoudi, H. Deformation of bulk dielectric fluids under corona-initiated charge injection. *Exp. Fluids* **2020**, *61*, No. 116.
(33) Chang, J.-S.; Lawless, P. A.; Yamamoto, T. Corona discharge processes. *IEEE Trans. Plasma Sci.* **1991**, *19*, 1152−1166.
(34) Robinson, M. Movement of air in the electric wind of the corona discharge. *Trans. Am. Inst. Electr. Eng., Part I: Commun. Electron.* **1961**, *80*, 143−150.
(35) Goldman, M.; Goldman, A.; Sigmond, R. The corona discharge, its properties and specific uses. *Pure Appl. Chem.* **1985**, *57*, 1353−1362.
(36) Hosseini, M.; Shahavi, M.; Yakhkeshi, A. AC & DC-currents for separation of nano-particles by external electric field. *Asian J. Chem.* **2012**, *24*, 181−184.
(37) Abd Rahman, N.; Ibrahim, F.; Yafouz, B. Dielectrophoresis for biomedical sciences applications: A review. *Sensors* **2017**, *17*, No. 449.
(38) Obukhov, Y. N.; Hehl, F. W. Electromagnetic energy−momentum and forces in matter. *Phys. Lett. A* **2003**, *311*, 277−284.
(39) Onsager, L. Deviations from Ohm's law in weak electrolytes. *J. Chem. Phys.* **1934**, *2*, 599−615.
(40) Fridman, A. *Plasma Chemistry*; Cambridge University Press, 2008.
(41) Csele, M. *Fundamentals of Light Sources and Lasers*; John Wiley & Sons, 2011.
(42) Fridman, A.; Chirokov, A.; Gutsol, A. Non-thermal atmospheric pressure discharges. *J. Phys. D: Appl. Phys.* **2005**, *38*, No. R1.
(43) Sheikholeslami, M. Investigation of Coulomb force effects on ethylene glycol based nanofluid laminar flow in a porous enclosure. *Appl. Math. Mech.* **2018**, *39*, 1341−1352.
(44) Shahbaznezhad, M.; Dehghanghadikolaei, A.; Sojoudi, H. Contactless Method for Electrocoalescence of Water in Oil. *ACS Omega* **2021**, *6*, 14298−14308.
(45) Shahbaznezhad, M.; Dehghanghadikolaei, A.; Sojoudi, H. Optimum Operating Frequency for Electrocoalescence Induced by Pulsed Corona Discharge. *ACS Omega* **2020**, *5*, 31000−31010.
(46) Mohr, P. J.; Taylor, B. N.; Newell, D. B. CODATA recommended values of the fundamental physical constants: 2006. *J. Phys. Chem. Ref. Data* **2008**, *80*, No. 1187.
(47) Purcell, E. M.; Morin, D. J. *Electricity and Magnetism*; Cambridge University Press, 2013; Vol. *I*.
(48) O'Brien, R. W.; White, L. R. Electrophoretic mobility of a spherical colloidal particle. *J. Chem. Soc., Faraday Trans. 2* **1978**, *74*, 1607−1626.
(49) Li, B.; Vivacqua, V.; Wang, J.; Wang, Z.; Sun, Z.; Wang, Z.; Ghadiri, M. Electrocoalescence of water droplets in sunflower oil using a novel electrode geometry. *Chem. Eng. Res. Des.* **2019**, *152*, 226−241.
(50) Chen, Q.; Ma, J.; Xu, H.; Zhang, Y. The impact of the ionic concentration on electrocoalescence of the nanodroplet driven by dielectrophoresis. *J. Mol. Liq.* **2019**, *290*, No. 111214.
(51) Im, D. J.; Noh, J.; Yi, N. W.; Park, J.; Kang, I. S. Influences of electric field on living cells in a charged water-in-oil droplet under electrophoretic actuation. *Biomicrofluidics* **2011**, *5*, No. 044112.
(52) Lu, Q.; Terray, A.; Collins, G. E.; Hart, S. J. Single particle analysis using fluidic, optical and electrophoretic force balance in a microfluidic system. *Lab Chip* **2012**, *12*, 1128−1134.
(53) Tabuteau, H.; Coussot, P.; de Bruyn, J. R. Drag force on a sphere in steady motion through a yield-stress fluid. *J. Rheol.* **2007**, *51*, 125−137.
(54) Zhu, T.; Yang, W. Toughness variation of ferroelectrics by polarization switch under non-uniform electric field. *Acta Mater.* **1997**, *45*, 4695−4702.
(55) Henson, B. L. A derivation of Warburg's law for point to plane coronas. *J. Appl. Phys.* **1981**, *52*, 3921−3923.
(56) Warburg, E. *Handbuch der Physik*; Springer, 1927; Chapter 14, pp 154−155.
(57) Starrett, C. E. Coulomb log for conductivity of dense plasmas. *Phys. Plasmas* **2018**, *25*, No. 092707.
(58) Kamra, A.; Deshpande, C.; Gopalakrishnan, V. Effect of relative humidity on the electrical conductivity of marine air. *Q. J. R. Meteorol. Soc.* **1997**, *123*, 1295−1305.
(59) Zhang, H.; Chen, X.; Cao, F.; Wang, G.; Dong, X.; Hu, Z.; Du, T. Charge−discharge properties of an antiferroelectric ceramics capacitor under different electric fields. *J. Am. Ceram. Soc.* **2010**, *93*, 4015−4017.
(60) Uman, M. A.; McLain, D. K.; Fisher, R. J.; Krider, E. P. Electric field intensity of the lightning return stroke. *J. Geophys. Res.* **1973**, *78*, 3523−3529.
(61) Sepehri, A.; Pincak, R.; Bamba, K.; Capozziello, S.; Saridakis, E. N. Current density and conductivity through modified gravity in the graphene with defects. *Int. J. Mod. Phys. D* **2017**, *26*, No. 1750094.
(62) Halliday, D.; Resnick, R.; Krane, K. S.; Stanley, P. *Physics*; Wiley, 2001; Vol. *1*.
(63) Wilm, M. S.; Mann, M. Electrospray and Taylor-Cone theory, Dole's beam of macromolecules at last? *Int. J. Mass Spectrom. Ion Processes* **1994**, *136*, 167−180.
(64) Zhang, Y.; Zhang, P.; Ma, B.; Wu, H.; Zhang, S.; Xu, X. Sewage sludge disintegration by high-pressure homogenization: a sludge disintegration model. *J. Environ. Sci.* **2012**, *24*, 814−820.
(65) Gul, O.; Saricaoglu, F. T.; Mortas, M.; Atalar, I.; Yazici, F. Effect of high pressure homogenization (HPH) on microstructure and rheological properties of hazelnut milk. *Innovative Food Sci. Emerging Technol.* **2017**, *41*, 411−420.
(66) Li, W.; Leong, T. S.; Ashokkumar, M.; Martin, G. J. A study of the effectiveness and energy efficiency of ultrasonic emulsification. *Phys. Chem. Chem. Phys.* **2018**, *20*, 86−96.
(67) Suvorov, V. G.; Zubarev, N. M. Formation of the Taylor cone on the surface of liquid metal in the presence of an electric field. *J. Phys. D: Appl. Phys.* **2004**, *37*, 289.
(68) Fernández de la Mora, J. The fluid dynamics of Taylor cones. *Annu. Rev. Fluid Mech.* **2007**, *39*, 217−243.

https://doi.org/10.1021/acsomega.1c06765
ACS Omega 2022, 7, 7045−7056